Variable symbol-rate DPSK receiver based on silicon photonics coupled-resonator delay line

Marco Mattarei, Antonio Canciamilla, Stefano Grillanda, and Francesco Morichetti, *IEEE Member*

I. Introduction

Differential phase-shift keying (DPSK) optical transmission systems offer several advantages over on-off keying (OOK) systems in terms of tolerance to fiber chromatic dispersion and nonlinearities, increased robustness to narrow optical filtering, and 3-dB improvement of the receiver sensitivity when combined with balanced detection [1]. Direct-detection of DPSK signals requires the conversion of phase modulation to intensity modulation, which is usually performed by means of Mach-Zehnder interferometers (MZI) with a fixed delay equal to the inverse of the signal symbol rate (e.g. 100 ps delay at 10 Gsym/s) [2]. However, the detection of DPSK signals affected by bandwidth-narrowing due to concatenated filters [3] or by chromatic dispersion [4] may be improved if the delay at the receiver deviates from the one-symbol delay. Furthermore, receivers capable of demodulating signals at variable symbol-rates would better fulfill the requirements of optical communication systems, which are evolving toward gridless schemes with higher channel flexibility and dynamic bandwidth allocation [5].

A possible approach is to use constant-delay microring resonators as DPSK receivers, which have been demonstrated to be more robust to symbol-rate variations compared to constant-delay MZI receivers [6]. However, in these schemes some power penalty is inherently observed when the symbol-rate deviates from the optimum value. Therefore, variable delay DPSK receivers have been attracting an increasing interest. Several solutions have been proposed in free-space [7] and optical fiber [8] technologies: however, while offering large delay tunability and good optical performance, these devices are bulky and expensive. An integrated solution for an interferometer with adaptive delay has been realized by using cascaded MZIs [9], yet this device provides only a discrete switching between three delays. More recently Suzuki *et al.* have demonstrated an integrated silicon photonics differential quadrature PSK (DQPSK) receiver, where the delay can be varied through an all-pass microring slow-light architecture [10]. In this device, tunability from 7.4 to 9 Gsym/s was achieved by individually controlling the resonance of 10 microring resonators.

In this work we demonstrate a simpler approach to realize an integrated variable symbol-rate receiver for DPSK optical systems. The variable delay is attained by means of a coupled resonator optical waveguide (CROW) inserted in one arm of a conventional unbalanced MZI. The fabricated device is realized in silicon-on-insulator (SOI) technology and can be tuned to optimally detect DPSK signals at any symbol rates between 9.8 and 15 Gsym/s.

II. Device Concept

As shown in the schematic of Fig. 1(a), the proposed device consists of an unbalanced MZI with a tunable delay line coupled with the longer arm of the interferometer. The delay line, consisting of a tunable CROW in reflective configuration, is used to modify the mutual delay between the two arms of the MZI in order to adapt the receiver bandwidth to the symbol rate of the incoming DPSK signal. Figure 1(a) shows the case of a MZI coupled with a three-ring CROW, but the proposed concept applies to an arbitrary number of resonators.

Manuscript received…
This work was supported in part by the Italian PRIN 2009 project Shared Access Platform to Photonic Integrated Resources (SAPPHIRE) and by the FP7-ICT European FET Project BBOI (www.bboi.eu).

M. Mattarei, S.Grillanda and F. Morichetti are with the Dipartimento di Elettronica, Informazione e Bioingegneria - Politecnico di Milano, via Ponzio 34/5, francesco.morichetti@polimi.it)

A. Canciamilla is now with Cisco Systems, via Philips 12, 20900 Monza MB, Italy.

Color versions of one or more of the figures in this letter are available online.

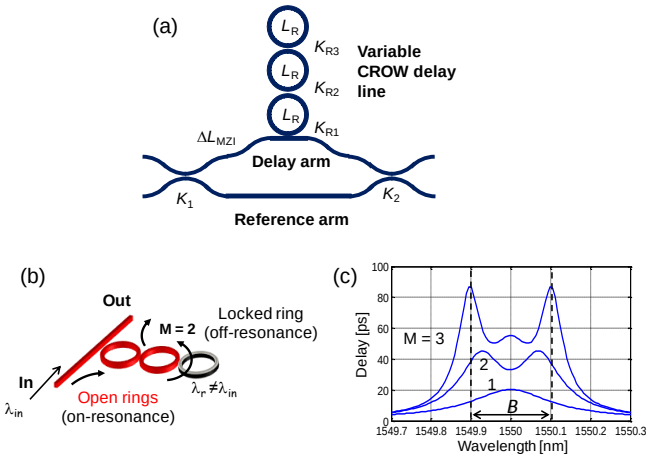

Fig. 1. (a) Schematic of the variable delay DPSK receiver consisting of an unbalanced MZI loaded with a tunable CROW delay line. (b) Delay tuning mechanism of a reflective CROW delay line. (c) Simulated group delay of the CROW delay line when M rings (M = 1, 2, 3) are progressively set to resonance.

The working principle of a tunable CROW delay-line is discussed in [11] and is here briefly summarized referring to Fig. 1(b). If the spectrum of the incoming signal, that is assumed to be centered at wavelength λ_{in} does not overlap with the transmission bandwidth B of the CROW, the signal is not coupled to the CROW and propagates in the bus waveguide only. In these conditions, the relative delay between the MZI arms is minimum and provides the maximum attainable free spectral range $FSR_{max} = c/(n_g \Delta L_{MZI})$ of the receiver, where ΔL_{MZI} is the geometric unbalance between the two arms of the MZI, c is the vacuum light speed and n_g is the waveguide group index.

If λ_{in} falls within the transmission bandwidth of the CROW, the incoming signal can propagate through the delay line provided that its bandwidth does not exceed B. The delay provided by the CROW can be increased by setting the resonant wavelength λ_{Ri} of an increasing number M of adjacent resonators to λ_{in}. In a CROW with identical resonators with the same coupling coefficients K_{Ri}, each ring provides a delay comprised between 0 (*locked ring*, off-resonance condition) and

$$T_{max} = \frac{2}{\pi B}, \qquad (1)$$

that is the delay due to the double pass light propagation across a ring in on-resonance condition (*open ring*). By partially detuning the resonance of the last open ring, any intermediate delay between 0 and T_{max} can be added in order to control the overall delay with continuity [11]. In previous contributions we demonstrated that the continuous control of the delay by tuning the last ring into partial resonance does not affect significantly the quality of either intensity [11] or phase [12] modulated signals.

Actually, the need for impedance matching of the CROW to the bus waveguide requires that K_{Ri} progressively decrease (that is the finesse of the resonators increases) along the structure [13], so that the maximum delay provided by each resonator slightly deviates from the mean value T_{max} provided by Eq. (1). For example, Fig. 1(c) shows the simulated group delay of a tunable CROW delay line made of 3 identical coupled resonators with geometric length L_R = 476 μm, n_g = 4.2, and FSR = $c/(n_g L_R)$ = 150 GHz. The coupling coefficients (K_{R1} = 0.76, K_{R2} = 0.26, and K_{R3} = 0.15) are designed in order to provide a bandwidth B of about 25 GHz. The additional delay provided by each open ring, averaged across the CROW passband, is 17 ps (M = 1), 22 ps (M = 2), and 23 ps (M = 3). The tuning approach, which is here numerically shown for 3 rings only, can be generalized to an arbitrary number of coupled rings [14].

The group delay of the CROW is not constant across the transmission band B and exhibits two sharp peaks at the band edges. Moreover, some ripples are originated by the interference of the delayed optical signal with the small fraction of the light that is not coupled with the CROW (about 5% in the considered example). However, no significant distortion occurs in the delayed signal provided that the group delay variations across the signal bandwidth are small. This condition is achieved if the impedance matching of the structure is optimized and if the signal spectrum is entirely contained within the CROW passband [11].

III. Device Fabrication and Characterization

The proposed device was fabricated on a SOI platform with a 2-μm thick oxide buffer layer [15]. Waveguides are written on a hydrogen silsesquioxane (HSQ) resist through electron-beam lithography followed by an inductively coupled plasma etching process. The waveguide core has a rectangular shape, with 220 nm thickness and 480 nm width, and is covered with a 1-μm-thick oxide layer. Inversely tapered waveguide sections, buried in a SU-8 polymer waveguide, were realized at the chip facets to reduce the coupling loss with optical fibers.

The top view photograph of a fabricated device is shown in Fig. 2. The MZI unbalance is ΔL_{MZI} = 4736 μm and the longer arm is folded in order to keep the overall footprint as small as 900 μm × 700 μm. To minimize radiation loss in the bends and at the straight-to-curved waveguide transitions, the minimum curvature radius of the circuit is larger than 20 μm. A CROW made of two microring resonators is coupled to the longer arm of the MZI. The rings have a racetrack geometry

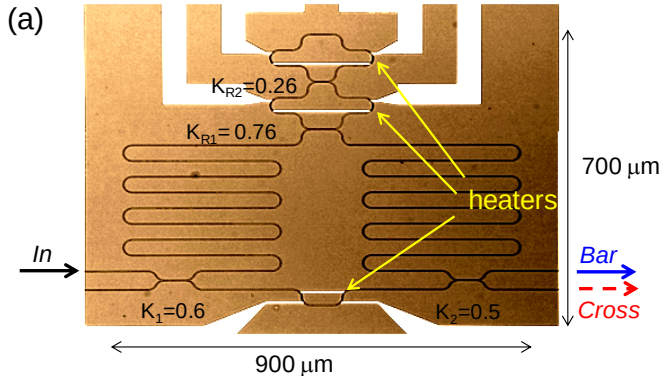

Fig. 2. Top-view photograph of the silicon photonics variable symbol-rate DPSK receiver.

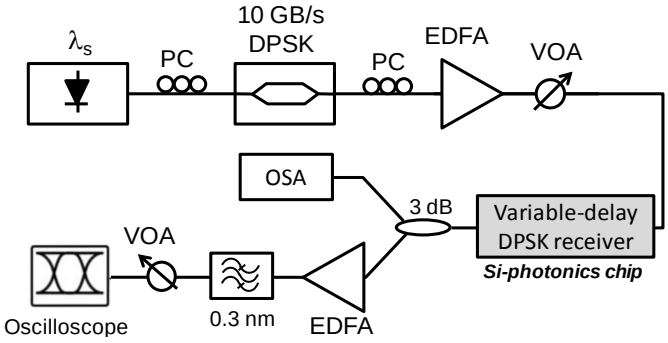

Fig. 3. Schematic of the experimental setup employed for the characterization of the variable symbol-rate DPSK receiver.

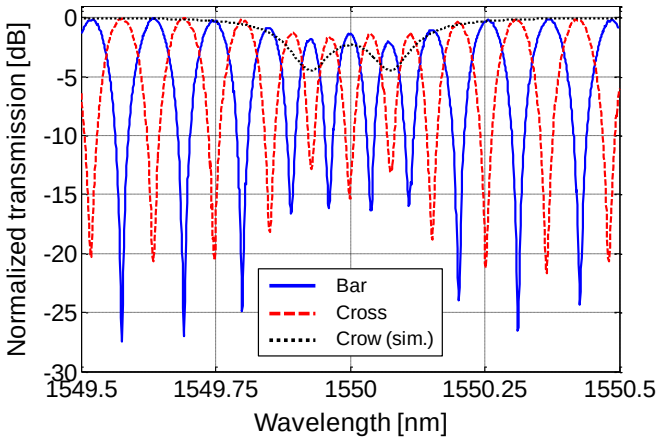

Fig. 4. Measured transmission of the device at the Bar port (blue solid curve) and at the Cross port (red dashed line) when both rings resonate at 1550 nm. The black dashed curve shows the simulated transmission of the CROW in the same tuning condition.

with the same design parameters of the first two rings of the device considered in Fig. 1(c), that is L_R = 476 μm, K_{R1} = 0.76 and K_{R2} = 0.26. The directional couplers of the rings have a gap distance between the waveguide of 300 nm, and a coupling length of 26 μm and 56 μm, respectively. The power coupling coefficients of the MZI directional couplers, K_1 = 0.6 and K_2 = 0.5, were optimized to compensate for the delay-dependent loss of the CROW in order to guarantee a good extinction ratio (ER) of the MZI response at any tuning conditions (see Sec. V.A). Metallic heaters were deposited onto the waveguides to thermally adjust the resonant wavelengths λ_{R1} and λ_{R2} of the rings [16], and to finely set the phase of the reference arm of the MZI. The metal lines connecting the heaters to the contact pads consist of a 200 nm thick Au film deposited onto the silica cladding with an intermediate 20 nm thick Ti adhesion layer.

IV. Experimental Setup

Figure 3 shows the experimental setup used for the optical characterization of the proposed device and for evaluating its performance on the detection of DPSK signals. A tunable laser is employed to generate a continuous-wave (CW) optical signal at a wavelength λ_s around 1550 nm. The light source is modulated with a $LiNbO_3$ phase modulator driven by a 10 Gb/s signal. The modulated signal is then amplified by an erbium-doped fiber amplifier (EDFA) and its intensity is controlled through a variable optical attenuator (VOA). Two polarization controllers (PCs) are used to adjust the polarization of the light at the input of the modulator and of the chip, respectively. Tapered lensed fibers with 1.7 μm spot size were employed to couple the light into and out of the silicon chip. The state of polarization is set to TE and the coupling loss of the inverse taper is about 5 dB.

In order to perform simultaneous time domain and frequency domain measurements, at the output of the chip a 3 dB fiber coupler is employed to transmit a portion of the signal to an optical spectrum analyzer (OSA) and to a 20 GHz optical sampling oscilloscope. Due to the limited sensitivity of the oscilloscope used for eye diagram measurements (about −15 dBm), a second EDFA is used to compensate for the insertion loss of the chip (about 12 dB) and a VOA is added to keep a constant power level of about -9 dBm at the input of the photodiode. The signal is also filtered using a tunable band pass filter with a bandwidth of 0.3 nm to remove the off-band amplified spontaneous emission (ASE) noise generated by the two EDFAs.

V. Experimental Results

A. Spectral response and delay tuning

The measured spectral response at the two output ports of the fabricated device is shown in Fig. 4, when the resonant wavelengths of both rings are tuned at the same wavelength λ_0 = 1550 nm. Referring to Fig 2, the blue solid curve shows the transmission at the Bar port, while the red dashed curve is the transmission at the Cross port. The simulated intensity transmission of the CROW in this tuning condition is shown by the black dashed curve. At wavelengths outside the CROW transmission band (for instance between 1549.5 nm and 1549.8 nm) the delay of the CROW is almost zero, and the receiver exhibits the maximum attainable FSR of 15 GHz, corresponding to the delay T_{MZI} = 66.7 ps between the waveguides of the MZI arms. Around λ_0, the CROW adds a delay of about 34.5 ps [see Fig. 1(c)], that reduces the FSR to the minimum value of 9.8 GHz. Since the delay of the CROW can be continuously tuned between 0 and 34.5 ps, any intermediate FSR can be achieved at the desired wavelength.

Figure 5(a) shows the tunability of the device transmission spectrum around λ_0. Let us assume as initial condition that both rings are off-resonance, that is $\lambda_{R1} \neq \lambda_0$ and $\lambda_{R2} \neq \lambda_0$ (blue curve, FSR = 15 GHz). Starting from this condition, the resonance λ_{R1} of the first ring is tuned to λ_0, thus reducing the FSR of the device to 11.54 GHz (green curve). Then, by having also the second ring resonate at $\lambda_{R2} = \lambda_0$, the FSR is further reduced to 9.8 GHz (red curve). Figure 5(b) shows the measured delay (red circles) between the MZI arms at several tuning conditions between the minimum and maximum attainable FSR. Continuous delay tunability is achieved from 66.6 ps to 102 ps, enabling the use of the receiver for the optimal detection of DPSK signals with a symbol rate spanning from 9.8 to 15 Gsym/s (blue squares). Here, a fractional number *M* means that the last open ring is set to an intermediate condition between on-resonance and off-

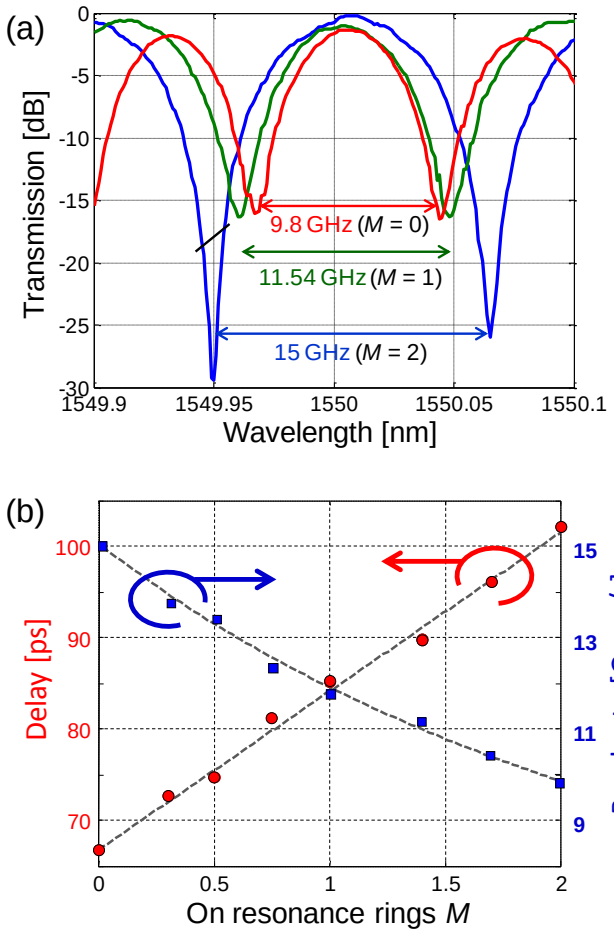

Fig. 5. (a) Measured transmission of the variable delay MZI when both rings are off-resonance (blue curve, $\lambda_{R1} = \lambda_{R2} = 1550.6$ nm, FSR = 15 GHz), only the first ring is on resonance (green curve , $\lambda_{R1} = 1550$ nm, $\lambda_{R2} = 1550.6$ nm, FSR = 11.54 GHz), and both rings are on resonance (red curve, $\lambda_{R1} = \lambda_{R2} = 1550$ nm, FSR = 9.8 GHz). (b) The receiver delay (red circles) and symbol-rate (blue squares) are continuously tuned from 66 ps (15 Gsym/s) to 102 ps (9.8 Gsym/s) by shifting the rings resonances.

resonance state. For instance, in the case $M = 1.7$, the first ring is set to resonance ($\lambda_{R1} = \lambda_0$), while the second ring is partially detuned from resonance, in such a way that its group delay is 70% of the maximum delay that the ring can provide when $\lambda_{R2} = \lambda_0$. The relation between the delay and the partial detuning of the last ring of CROW delay lines was discussed in [11]. Once the required detuning is known, the electric power driving the thermooptic actuator can be adjusted to achieve the desired delay.

Figure 5(a) shows that the FSR decrease is associated with a reduction of the ER of the receiver. This effect is mainly due to the delay-dependent loss of the CROW. The round trip loss of the ring resonators was estimated around 0.35 dB/turn, where 0.15 dB loss is due to the waveguide propagation loss (3 dB/cm), and 0.2 dB loss is from the excess loss of the directional couplers and the straight-curve transitions in the resonator geometry. Nonetheless, an ER higher than 15 dB was observed at any tuning conditions between the minimum and maximum FSR. In a single-ended receiver, the expected power penalty due to non-infinite ER is less than 0.5 dB for

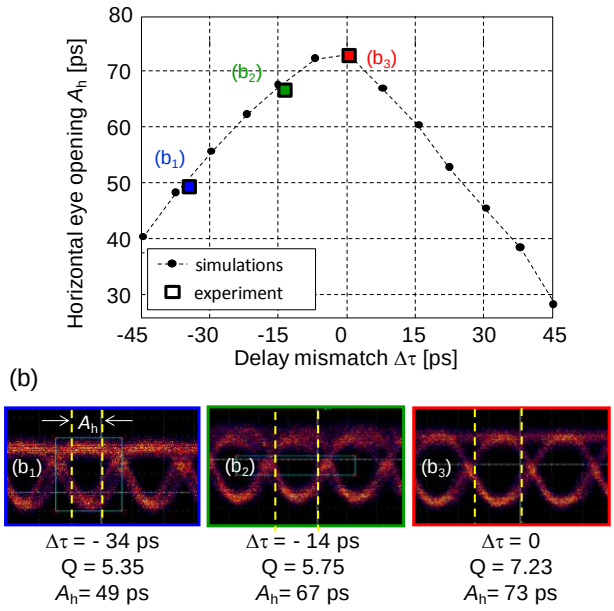

Fig. 6. Performance of the variable delay DPSK receiver for a 10 Gsym/s signal. Simulated (circles) and measured (squares) horizontal opening A_h of the detected eye-diagram versus the mismatch Δτ between the MZI delay and the symbol time. Measured eye diagrams are shown in (b).

ER >15 dB, while in a balanced detection scheme is almost negligible [2]. The total on-chip insertion loss of the device is slightly affected by the delay-dependent loss of the CROW, since it increases from 1 dB to 2 dB loss from the maximum to the minimum FSR condition.

Full tunability of the receiver requires that the ring round trip phase is shifted from 0 to π to bring the resonators from off-resonance to on-resonance state. An additional phase shift of up to π is required in the shorter arm of the MZI to align the receiver response to the wavelength of the transmitted signal. As in conventional MZIs, a π phase-shift between the MZI arms is responsible for the half FSR shift of the spectral response, that is for the mutual switch of the Bar and Cross ports. Since the power consumption of the fabricated heaters is 10 mW to achieve π-shift, less than 30 mW are needed for the full tunability of the receiver. However, several optimized geometries have been proposed to increase the thermal efficiency of the heaters [17,18], which can be adopted to further reduce the power consumption of the device.

B. DPSK signal detection

The variable delay MZI was employed to receive a 10 Gsym/s binary DPSK signal transmitted at a wavelength of 1550 nm. In particular, in our experiment, the delay of the CROW was optimized to match the exact symbol rate of the signal and optimize the performance of the system. The quality of the detected signal was evaluated by considering the system Q-factor and the half-height horizontal opening A_h of the eye diagram, the latter providing direct information on the impairments associated with intersymbol interference (ISI) effects.

Figure 6(a) shows the comparison between the simulated (circles) and measured (squares) A_h of the intensity modulated

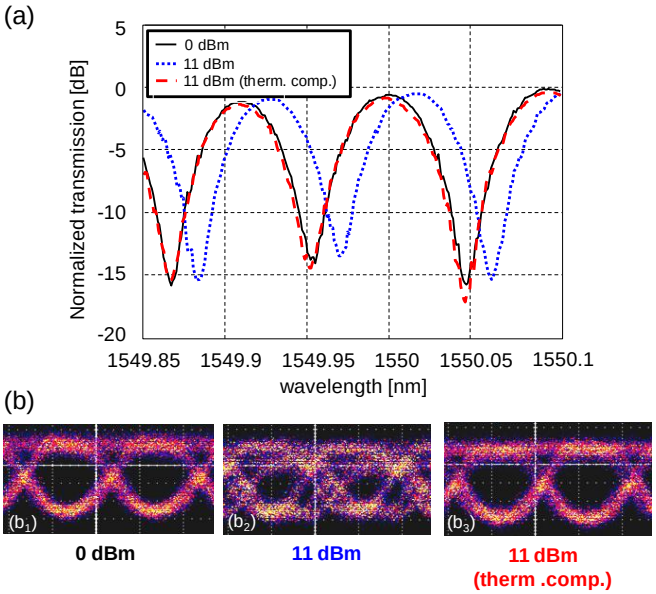

Fig. 7. (a) Frequency-domain response of the variable delay receiver optimized for the detection of a 10 Gsym/s DPSK signal for increasing power in the input waveguide: 0 dBm (black solid curve), 11 dBm (blue dotted curve). The red dashed curve shows the thermally compensated nonlinear response. (b) Eye diagrams of the detected signal when the receiver operates in the three conditions shown in (a).

signal detected in single-ended configuration versus the delay mismatch $\Delta\tau$ between the MZI delay and the symbol time. Simulations were performed by using the measured spectral response of the MZI receiver and assuming a noise-free optical signal. When the two rings are tuned off-resonance, the symbol rate does not match the FSR of the receiver (FSR = 15 GHz) and $\Delta\tau$ = -34 ps (blue square). In these conditions, the measured eye-diagram [shown Fig. 6(b_1)] is triangularly shaped because of the strong ISI that causes an evident splitting of the signal transitions. The eye opening A_h is as low as 49 ps and the Q-factor is 5.35.

By opening the first ring (λ_{R1} = 1550 nm), $\Delta\tau$ is reduced to -14 ps, transition splitting in the detected eye diagram disappears (b_2), and A_h increases to 67 ps (green square). Full delay-mismatch compensation ($\Delta\tau = 0$) is obtained when the second ring is partially opened (λ_{R2} about 1549.82 nm) and the detected eye diagram (b_3) exhibits the maximum opening A_h = 73 ps (red square) and a Q-factor of more than 7. In these conditions, the amplitude modulation depth of the demodulated signal is more than 10 dB. The absence of ISI in the eye-diagram after full compensation of the delay mismatch demonstrates that the non-ideally flat group delay of the CROW does not introduce any significant degradation in the detected signal.

The results refer to the receiver used in single-ended configuration. However, as shown in Fig. 4, within the CROW passband the proposed device behaves as a conventional MZI, that is constructive interference at one output port implies destructive interference at the other port. Therefore, balanced detection can be adopted to improve receiver performance.

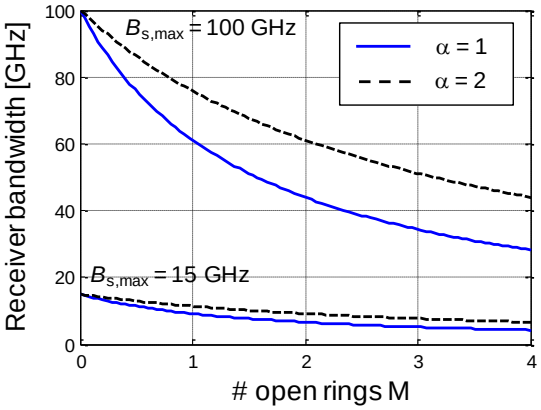

Fig. 8. Tunability range of the variable-symbol rate receiver versus the number of open rings loaded to the longer arm of the MZI. Maximum receiver bandwidths (M=0) of 15 and 100 GHz are considered. Blue solid curves indicate the case $B = B_s$ (α = 1), black dashed curves indicate the case $B = 2B_s$ (α = 2).

C. *Robustness to nonlinear effects*

The variable delay DPSK receiver was also tested at high input power to evaluate the impact of nonlinear effects on the detected signal. The receiver was first calibrated in the linear regime to have the best performance ($\Delta\tau = 0$) for a 10 Gsym/s signal. Black curve in Fig. 7(a) shows the device transmission when the power in the input waveguide of the receiver is 0 dBm and the detected eye is shown in Fig. 7(b_1). When the input power is increased to 11 dBm, thermal effects induced by two-photon absorption (TPA) introduce a distortion of the device transmission [16], that mainly consists of a 22 pm red-shift of the spectral response (blue dotted curve). As shown in Fig. 7(b_2), this misalignment between the receiver and the signal carrier frequencies causes a strong distortion of the eye-diagram. The nonlinear red-shift can be easily compensated by adjusting the temperature of the integrated heaters in order to make the high power spectral response overlap the calibrated linear response (red dashed curve) and restore the eye diagram [see Fig 7(b_3)].

VI. Discussion

The symbol-rate variability range of the receiver discussed in Sec. V was designed in order to provide a proof-of-concept demonstration of the device performance with the 10 Gbit/s measurement facilities available in our lab. However, silicon photonics enables the scalability of the proposed receiver to up 100 Gsym/s systems and beyond.

A variable symbol-rate DPSK receiver operating from 40 to 100 Gsym/s can be realized with a MZI unbalance ΔL_{MZI} = 714 μm (providing a delay of 10 ps, corresponding to FSR_{max} = 100 GHz) and a CROW with B = 100 GHz. A 100 GHz bandwidth can be obtained with ring resonators with a FSR of 600 GHz and the same coupling coefficients K_{Ri} used in Fig. 1(c). The corresponding geometric length of the rings (120 μm) requires a bending radius of more than 15 μm, that is achievable with silicon photonics waveguides with no significant bending loss. With these design parameters, the delay provided by each ring is 4.6 ps (M = 1), 5.5 ps (M = 2),

and 5.7 ps (M = 3), thus providing delay tunability from 10 ps to about 26 ps, corresponding to a bandwidth tunability from 100 GHz to less than 40 GHz.

The maximum tunability range achievable with the proposed receiver can be simply related to the number of rings loaded to the longer arm of the MZI. In fact, the ratio between the maximum and minimum bandwidth of the receiver, respectively given by the maximum and minimum FSR of the ring-loaded MZI, is given by

$$\frac{FSR_{\max}}{FSR_{\min}} = \frac{T_{MZI} + T_{CROW,\max}}{T_{MZI}} = 1 + \frac{MT_{\max}}{T_{MZI}}, \qquad (2)$$

where $T_{\mathrm{CROW,max}}$ is the maximum delay provided by a CROW with M rings set to resonant condition (open rings). Actually, Eq. (2) rigorously holds for a CROW with M identical resonators, each one providing a delay $T_{\max}$ given by Eq. (1). However, as shown in the numerical example discussed in Sec. II, the relation $T_{\mathrm{CROW,max}} = MT_{\max}$ can provide a good estimate of the total delay of an impedance-matched CROW with M resonators of increasing finesse.

Both the fixed delay T_{MZI} between the MZI arms and the delay $T_{\max}$ given by each ring depend on the bandwidth B_{s} of the signal to be detected. In fact, T_{MZI} has to be chosen in order to exactly match the maximum signal bandwidth, that is $T_{\mathrm{MZI}}=B_{\mathrm{s,max}}^{-1}$. Then, in order to avoid significant distortion of the detected signal, $B_{\mathrm{s,max}}$ has to be smaller than the CROW bandwidth B, that is $T_{\max} = 2/\alpha\pi B_{\mathrm{s,max}}$, where the $\alpha = B/B_{\mathrm{s,max}}$ (with $\alpha>1$). By substituting the conditions on T_{MZI} and $T_{\max}$ into eq. (2), one straightforwardly obtains

$$\frac{FSR_{\max}}{FSR_{\min}} == 1 + \frac{2M}{\alpha\pi}, \qquad (3)$$

relating the tunability range of the variable-symbol rate DPSK receiver to the number of rings of the CROW.

Figure 8 numerically shows the tunability range of receivers designed to have maximum bandwidths (M = 0) of 15 GHz and 100 GHz, respectively. By assuming $B = B_{\mathrm{s}}$ (blue solid curve, α = 1), the number of required rings is minimized and more than 50% bandwidth tunability is achieved with only 2 rings. However, this can result in some signal distortion originated by the band-edge peaks in the group delay response of the CROW [see Fig. 1(c)], especially when many rings are employed (M > 3). In fact when the number of rings is increased, the non-idealities of the group delay of the CROW may become more relevant, resulting in higher group delay peaks at the band edges and more pronounced in-band ripples. This implies that the ratio between the CROW bandwidth and the signal bandwidth has to be increased, in order to have no signal components propagating close to the band edge, and that the impedance matching must be also improved. In this view, tuning of the couplers may help the active optimization of the impedance matching, yet at the price of increasing control complexity and power dissipation.

In the device discussed in Sec. V, the bandwidth of the CROW (B = 25 GHz) was chosen about twice the signal bandwidth (black solid curve, α = 2), and no evidence of signal distortion was observed. Therefore, the α parameter has to be optimized, typically between values of 1 and 2, as a tradeoff between requirements on signal quality, electric power consumption for the tuning of the receiver and complexity of the tuning scheme, that increase with the number of rings to be controlled.

Some further comments are worthwhile about the loss of the device. As discussed in Sec. V.A, the 12 dB chip loss is essentially due to the coupling loss (5 dB/facet) from the fiber to the silicon waveguide. Optimized mode adaptors have been demonstrated to reduce the coupling loss to less than 1 dB per facet [19]. The 2 dB on-chip loss, resulting from the waveguide propagation loss (3 dB/cm) and from the excess loss of the directional couplers (0.2 dB) is expected to decrease to less than 1 dB by using state-of-the-art silicon nanowaveguides with less than 1 dB/cm [15, 20] and low loss directional coupler (<0.05 dB [21,22]). The delay-dependent loss essentially depends on the round trip loss of the ring (0.35 dB/turn in the current device), resulting in a loss of about 0.03 dB/ps. Ring resonators with roundtrip loss of about 0.1 dB/turn can be realized [21,22], thus reducing the delay dependent loss to less than 0.01 dB/ps and enabling to increase the delay tunability range.

A final consideration concerns the sensitivity of the device to the state of polarization of the incoming light. In our device, polarization sensitivity is related to the large birefringence of the silicon waveguides, and not to the device architecture. To mitigate polarization sensitivity in high index contrast waveguides, polarization diversity schemes can be adopted, where the polarization at the input of the chip is split into the orthogonal TE and TM components, and the TM component (typically) is rotated to TE in order to have only TE polarized light on chip [23, 24]. This is a general scheme that can be adopted for most devices and is applicable to the proposed receiver too.

VII. CONCLUSION

We presented a silicon photonics integrated DPSK receiver with continuously variable delay provided by a tunable CROW coupled to an arm of the interferometer. The device functionality was demonstrated by optimizing the detection of a 10 Gsym/s binary DPSK signal, but can be extended to generic DPSK systems with more complex data symbol constellations, for instance DQPSK, and to higher symbol rates. The delay of the fabricated receiver can be tuned between 66 ps and 102 ps, enabling detection of signals with a symbol-rate between 10 and 15 Gsym/s. The possibility to scale the approach to 100 Gsym/s systems has been also discussed.

Compared to alternative approaches, based for instance on a MZI loaded with microrings in all-pass filter configuration [10], the use of a CROW delay line in reflective configuration reduces the number of rings to be controlled, thus easing device reconfiguration and reducing power consumption [25]. The simplicity of the tuning scheme enables also to easily compensate thermal wavelength shifts induced by silicon nonlinearity at high input power.

Besides silicon photonics, the proposed device can be implemented on any photonic platforms enabling the realization of ring resonators, such as for instance high-index-contrast glass [11, 26, 27]. Finally, the possibility of

continuously controlling the delay of an integrated MZI can find applications also in different fields, such as pulse shaping techniques for semiconductor lasers [28], interferometer-based techniques for monitoring the quality of optical signals [29], and optical coherence tomography [30].

ACKNOWLEDGMENTS

The authors thank M. Strain, M. Sorel and the J. Watt Nanofabrication Centre (JWNC) staff at Glasgow University for the fabrication of the device, and A. Melloni, C. Ferrari, P. Orlandi, and P. Bassi for fruitful discussions.

REFERENCES

[1] A. H. Gnauck and P. J. Winzer, "Optical phase-shift-keyed transmission," *J. Lightwave Technol*., vol. 23, no 1, pp. 115-130, Jan. 2005.

[2] G. Bosco and P. Poggiolini, "On the joint effect of receiver impairments on direct-detection DQPSK systems," *J. Lightwave Technol*., vol. 24, no. 3, pp. 1323-1333, Mar. 2006.

[3] B. Mikkelsen, C. Rasmussen, P. Mamyshev, and F. Liu, "Partial DPSK with excellent filter tolerance and OSNR sensitivity," *Electron. Lett*., vol. 42, no. 23, pp. 1363-1364, Nov. 2006.

[4] Y. K. Lizé, L. Christen, X. Wu, J. Y. Yang, S. Nuccio, T. Wu, A. E. Willner, and R. Kashyap "Free spectral range optimization of return-to-zero differential phase shift keyed demodulation in the presence of chromatic dispersion," *Opt. Express*, vol. 15, no. 11, pp. 6817-6822, May 2007.

[5] O. Gerstel, M. Jinno, A. Lord, and S. J. B. Yoo, "Elastic optical networking: a new dawn for the optical layer?," *IEEE Communications Magazine*, vol. 50, no. 2, pp. s12-s20, Feb. 2012.

[6] K. Xu, G.K.P. Lei, S.M.G. Lo, Z. Cheng, C. Shu, and H.K. Tsang, "Bit-rate-variable DPSK demodulation using silicon microring resonators with electro-optic wavelength tuning," *IEEE Photon. Technol. Lett*., vol. 24, no. 14, pp. 1221-1223, July 2012.

[7] J. Li, K. Worms, R. Maestle, D. Hillerkuss, W. Freude, and J. Leuthold, "Free-space optical delay interferometer with tunable delay and phase," *Opt. Express*, vol. 19, no. 12, pp. 11654-11666, Jun. 2011.

[8] Y. Dai and C. Shu, "Bit-rate variable DPSK demodulation based on cascaded four-wave mixing," *Opt. Express*, vol. 19, no. 4, pp. 2952-2958, Feb. 2011.

[9] Y. Nasu, K. Hattori, T. Saida, Y. Hashizume, and Y. Sakamaki, "Silica-based adaptive-delay DPSK demodulator with a cascaded Mach-Zehnder interferometer configuration," *Proceed. 36th European Conference on Optical Communications*, Sept. 2010.

[10] K. Suzuki, H. Nguyen, T. Tamanuki, F. Shinobu, Y. Saito, Y. Sakai, and T. Baba, "Slow-light-based variable symbol-rate silicon photonics DQPSK receiver," *Opt. Express*, vol. 20, no. 4, pp. 4796-4804, Feb. 2012.

[11] F. Morichetti, A. Melloni, C. Ferrari, and M. Martinelli, "Error-free continuously-tunable delay at 10 Gbit/s in a reconfigurable on-chip delay-line," *Opt. Express*, vol. 16, no. 12, pp. 8395-8405, May 2008.

[12] A. Melloni, P. Boffi, C. Ferrari, L. Marazzi, F. Morichetti, R. Siano, M. Martinelli, "10-Gbit/s duobinary transmission controlled by a tunable coupled resonator optical delay line," Proceed. of Conference on Optical Fiber Communication (OFC 2009), San Diego, CA, March 22-26, 2009.

[13] A. Melloni and M. Martinelli, "Synthesis of direct-coupled-resonators bandpass filters for WDM systems," *J. Lightwave Technol*., vol. 20, no. 2, pp. 296-303, Feb. 2002.

[14] A. Melloni, A. Canciamilla, C. Ferrari, F. Morichetti, L. O'Faolain, T.F. Krauss, R. De La Rue, A. Samarelli, and M. Sorel, "Tunable delay lines in silicon photonics: coupled resonators and photonic crystals, a comparison," *IEEE Photon. Journal*, vol. 2, no. 2, pp. 181-194, Apr. 2010.

[15] M. Gnan, S. Thoms, D. S. Macintyre, R. M. De La Rue, and M. Sorel, "Fabrication of low-loss photonic wires in silicon-on-insulator using hydrogen silsesquioxane electron-beam resist," *Electron Lett*., vpl. 44, no. 2, pp. 115–116, Jan. 2008.

[16] A. Canciamilla, M. Torregiani, C. Ferrari, F. Morichetti, R. M. De La Rue, A. Samarelli, M. Sorel, and A. Melloni, "Silicon coupled-ring resonator structures for slow light applications: potential, impairments and ultimate limits," *J. Opt*., vol. 12, no. 10, 104008, Sep. 2010.

[17] P. Dong, W. Qian, H. Liang, R. Shafiiha, D. Feng, G. Li, J. E. Cunningham, A. V. Krishnamoorthy, and M. Asghari, "Thermally tunable silicon racetrack resonators with ultralow tuning power," *Opt. Express*, vol. 18, no. 19, pp. 20298-20304, Sep. 2010.

[18] Q. Fang; J. Song; X. Luo; L. Jia; M. Yu; G. Lo; Y. Liu, "High efficiency ring-resonator filter with NiSi heater," *IEEE Phot. Technol. Lett*., vol. 24, no. 5, pp.350-352, Mar. 2012.

[19] M. Pu, L. Liu, H. Ou, K. Yvind, and J. M. Hvam, "Ultra-low-loss inverted taper coupler for silicon-on-insulator ridge waveguide," *Opt. Communications*, vol. 283, no. 19, pp. 3678-3682, Oct. 2010.

[20] W. Bogaerts, and S. K. Selvaraja, "Compact single-mode silicon hybrid rib/strip waveguide with adiabatic bends," *IEEE Photonics Journal*, vol. 3, no. 3, pp. 422-432, June 2011.

[21] F. Xia, L. Sekaric, and Y. Vlasov, "Ultracompact optical buffers on a silicon chip," *Nat. Photon*., vol. 1 , no. 1, pp. 65-71, Jan. 2007.

[22] A. Melloni, A. Canciamilla, C. Ferrari, F. Morichetti, L. O'Faolain, T. F. Krauss, R. De La Rue, A. Samarelli, and M. Sorel, "Tunable delay lines in silicon photonics: coupled resonators and photonic crystals, a comparison," *IEEE Photonics Journal*, vol. 2, no.2, pp.181-194, April 2010.

[23] T. Barwicz, M. R. Watts, M. A. Popović, P. T. Rakich1, L. Socci, F. X. Kärtner, E. P. Ippen, and H. I. Smith, "Polarization-transparent microphotonic devices in the strong confinement limit," *Nat. Photonics*, vol. 1, pp. 57 – 60, Jan. 2007.

[24] H. Fukuda, K. Yamada, T. Tsuchizawa, T. Watanabe, H. Shinojima, and S. Itabashi, "Silicon photonic circuit with polarization diversity," *Opt. Express*, vol. 16, no. 7, pp. 4872-4880, Mar. 2008.

[25] A. Melloni, F. Morichetti, C. Ferrari, and M. Martinelli, "Continuously tunable 1 byte delay in coupled-resonator optical waveguides," *Opt. Lett*., vol. 33, no. 20, pp. 2389-2391, Oct. 2008.

[26] B. E. Little, S. T. Chu, P. P. Absil, J. V. Hryniewicz, F. G. Johnson, F. Seiferth, D. Gill, V. Van, O. King, and M. Trakalo, "Very high-order microring resonator filters for WDM applications," IEEE *Photon. Technol. Lett.*, vol. 16, no. 10, pp. 2263-2265, Oct. 2004

[27] T. Barwicz, M. Popovic, P. Rakich, M. Watts, H. Haus, E. Ippen, and H. Smith, "Microring-resonator-based add-drop filters in SiN: fabrication and analysis," *Opt. Express*, vol. 12, no. 7, pp. 1437-1442, Apr. 2004.

[28] A. Consoli and I. Esquivias, "Pulse shortening of gain switched single mode semiconductor lasers using a variable delay interferometer," *Opt. Express*, vol. 20, no. 20, pp. 22481-22489, Sep. 2012.

[29] F. Morichetti, A. Annoni, M. Sorel, and A. Melloni, A., "High-sensitivity in-band OSNR monitoring system integrated on a silicon photonics chip," *IEEE Photon. Technol. Lett*., vol. 25, no. 19, pp. 1939-1942, Oct. 2013.

[30] K. Takiguchi, M. Itoh, and H. Takahashi, "Integrated-optic variable delay line and its application to a low-coherence reflectometer," *Opt. Lett*., vol. 30, no. 20, pp. 2739-2741, Oct. 2005.